Polar Geosci., **12**, 29–48, 1999

DEFORMATION OF ULTRAHIGH-TEMPERATURE METAMORPHIC ROCKS FROM TONAGH ISLAND IN THE NAPIER COMPLEX, EAST ANTARCTICA

Tsuyoshi TOYOSHIMA[1], Yasuhito OSANAI[2], Masaaki OWADA[3], Toshiaki TSUNOGAE[4], Tomokazu HOKADA[5] and Warwick A. CROWE[6]

[1]*Graduate School of Science and Technology, Niigata University, Ikarashi, Niigata 950-2181*
[2]*Department of Earth Sciences, Faculty of Education, Okayama University, Tsushima-naka 3-chome, Okayama 700-8530*
[3]*Department of Earth Sciences, Yamaguchi University, Yoshida 1677–1, Yamaguchi 753-8512*
[4]*Faculty of Education, Shimane University, Nishi Kawatsu, Matsue 690-8504*
[5]*Department of Polar Science, School of Mathematical and Physical Sciences, The Graduate University for Advanced Studies, Kaga 1-chome, Itabashi-ku, Tokyo 173-8515*
[6]*Department of Geology and Geophysics, University of Western Australia, Nedlands, Perth 6907, Australia*

Abstract: The deformation history of ultrahigh-temperature metamorphic rocks from Tonagh Island, Napier Complex, East Antarctica is divided into nine stages, namely D_1 to D_9. The D_1 structure would have been formed under non- or weakly-deformational condition during thermal peak of prograde metamorphism. The D_2–D_6 structures would have been produced under retrograde granulite facies conditions. Subsequently D_7–D_9 brittle faulting modified the structures in part. The D_1 to D_8 deformation corresponds to first to third tectonometamorphic episodes, previously reported, of the whole Napier Complex before the intrusion of the Amundsen dyke.

The structural geology of the Island is mainly characterized by NE-SW trending D_2 foliation (S_2) with WNW plunging mineral lineation, WNW-ESE to E-W trending D_5 folds and NE-SW to E-W trending D_6 mylonite zones. S_2 is the main foliation of this area, but was highly folded and faulted during the D_5–D_6 stages. The S_2 and S_2-parallel D_3 shear zones are the products of layer-parallel shearing due to a top-to-the-SE (dextral-reverse) displacement. The D_3 and D_6 fault rocks show that seismic faulting and plastic deformation alternated both during the D_3 stage and during the D_6 stage under retrograde granulite facies conditions. Multiphase faulting in different shear senses occurred during the D_6 stage.

key words: Napier Complex, ultrahigh-temperature deformation, mylonite, foliated pseudotachylyte, deformation history

1. Introduction

Archean regional ultrahigh-temperature (UHT) metamorphic rocks, called the Napier Complex, widely crop out in northern Enderby Land, East Antarctica (*e.g.* SHERATON *et al.*, 1987). They are characterized by the occurrence of the rare associations of

spinel+quartz, sapphirine+quartz, sapphirine+garnet+quartz, orthopyroxene+sillimanite+quartz and osumilite within aluminous metasediments (*e.g.* SHERATON *et al.*, 1987), indicating UHT conditions of 1000–1100°C at 800–1000 MPa (HARLEY and HENSEN, 1990; HARLEY, 1998). The tectonometamorphic history of the Napier Complex has been established (SHERATON *et al.*, 1987), but is still in dispute (*cf.* OWADA *et al.*, 1994, 1996; SHIRAISHI *et al.*, 1997; ASAMI *et al.*, 1998). Many authors have described and discussed the structural geology and tectonic processes of UHT metamorphic rocks from the Napier Complex (JAMES and BLACK, 1981; SANDIFORD and WILSON, 1984; SANDIFORD, 1985; HARLEY, 1987; SHERATON *et al.*, 1987; TOYOSHIMA, *et al.*, 1998). However, nobody has so far reported on the structural geology of the UHT metamorphic rocks from Tonagh Island except for a small eastern island, East Tonagh Island (HARLEY, 1987).

The present authors have performed a detailed geological survey on Tonagh Island, in the central part of the Napier Complex, as members of the 39th Japanese Antarctic Research Expedition (1997–1998, JARE-39). This paper describes the structures of the UHT metamorphic rocks on Tonagh Island and discusses their deformation history. A movement picture of the UHT metamorphic rocks will also be synthesized in individual deformation stages.

2. Outline of Geology

Tonagh Island consists mainly of various kinds of metamorphic rocks (orthopyroxene-bearing quartzofeldspathic gneiss, garnet-bearing quartzofeldspathic gneiss, two-pyroxene-bearing mafic granulite, garnet-orthopyroxene gneiss and granulite, magnetite-quartz gneiss, two types of layered gneiss, and metamorphosed ultramafic rocks) with minor unmetamorphosed dykes (OSANAI *et al.*, 1999). The metamorphic rocks in the Island can be divided into five lithologic units (Units I to V, from north to south) on the basis of rock constitutions. Each unit is separated by NE-SW to E-W trending and steeply N dipping faults (unit boundary faults) associated with thick mylonite zones consisting of mylonite, foliated pseudotachylyte and pseudotachylyte (*cf.* OSANAI *et al.*, 1998, 1999). Metamorphosed and mylonitized mafic dykes which have two pyroxene-garnet assemblages occur in the mylonite zones.

The structural geology of the UHT metamorphic rocks is mainly characterized by NE-SW trending foliation with WNW plunging mineral lineation, WNW-ESE to E-W trending folds and NE-SW to E-W trending mylonite zones (Figs. 1 and 2). These were formed through the following poly-stage deformation.

3. Deformation History of Tonagh Metamorphic Rocks

The tectonism and metamorphism of a metamorphic belt are generally understood in terms of the *P-T-t-D* path of the constituent units. The first step of the *P-T-t-D* path analysis is to clarify the deformation history. The deformation history of ultrahigh-temperature metamorphic rocks from Tonagh Island is divided into nine stages, from D_1 to D_9, based on the characteristics of the deformation structures, deformation textures and movement pictures, as outlined in Table 1. The deformations of the D_1, D_2, D_3 and D_5 stages are penetrative on the geological-map scale, but those of the other stages (D_4 and

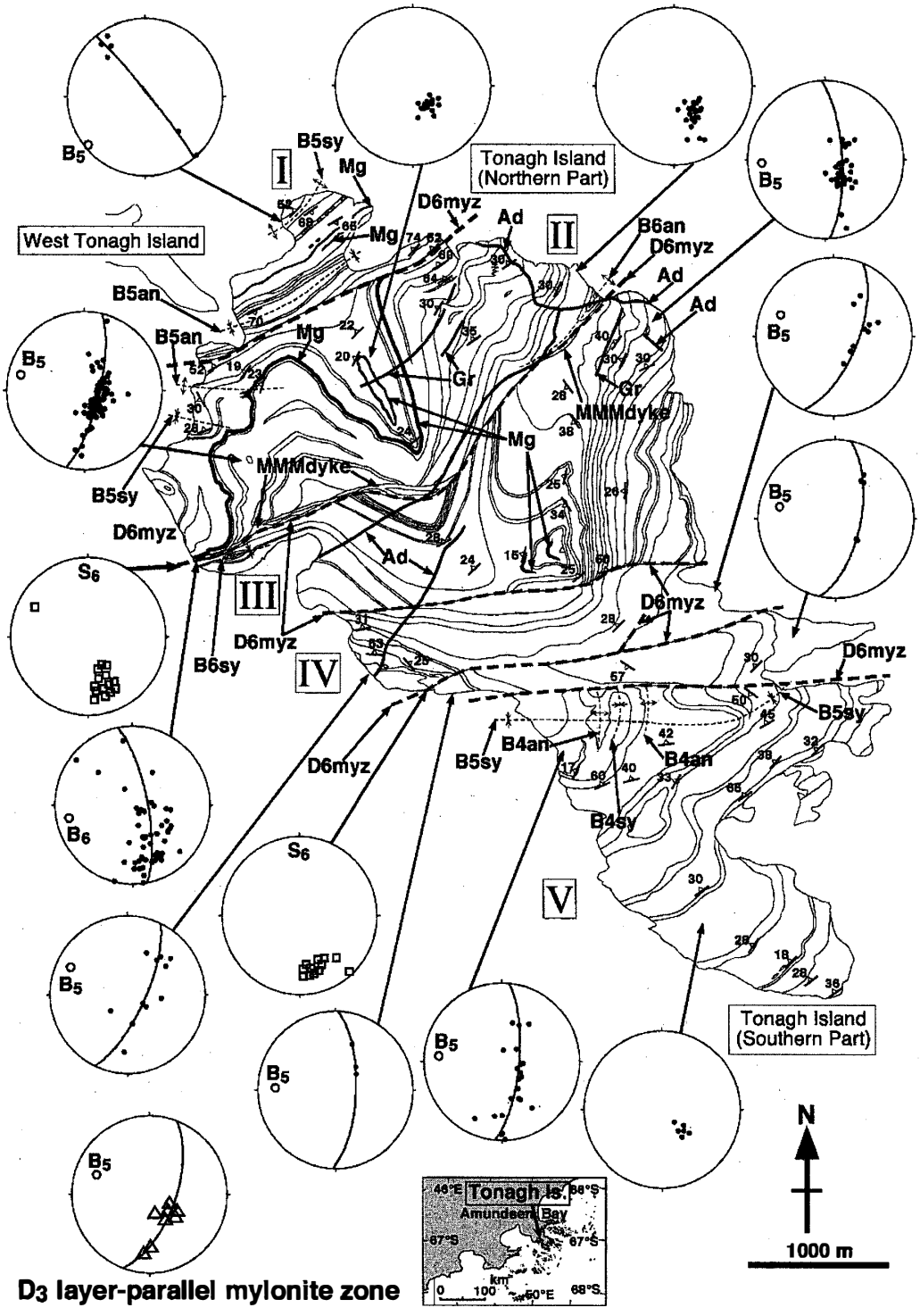

Fig. 1. Structural map and lower hemisphere equal area projections of poles to foliations (S_2:●, S_3:△, S_6:□) and to their best fit great circles (○, B_5, B_6) within Tonagh Island, modified from Osanai *et al. (1998, 1999). The poles (π axis) of these great circles express stereographically the orientations of the fold axes (B_5 and B_6). I, II, III, IV and V: lithologic units (*Osanai *et al., 1998, 1999). D6myz and thick broken line: D_6-mylonite zone, MMMdyke: D_6-metamorphosed and mylonitized mafic dyke, thick line: dykes (Ad: Amundsen dolerite dyke (D_9-dolerite dyke), Gr: D_9-pegmatite dyke) or magnetite-quartz gneiss (Mg), thin broken line: fold axis (B4an: B_4-antiform, B4sy: B_4-synform, B5an: B_5-antiform, B5sy: B_5-synform, B6an: B_6-antiform, B6sy: B_6-synform), thin line: lithologic boundary.*

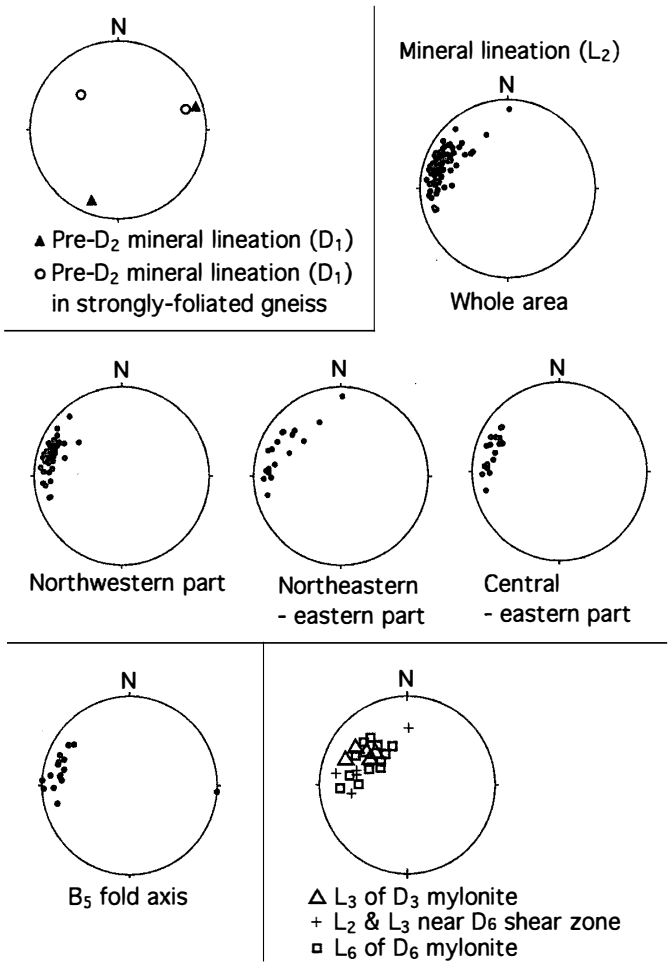

Fig. 2. Lower hemisphere equal area projections of pre-D_2, L_2, L_3 and L_6 mineral lineations and B_5 fold axes within Tonagh Island.

D_6 to D_9) are non-penetrative. Because each stage of deformation is associated with metamorphism and in some cases with magmatic intrusion, the deformation history is intimately related to the metamorphic and magmatic history. Some stages in the history are characterized by the occurrence of pseudotachylyte, which is formed by the frictional melting of rocks along fault surfaces during seismic faulting (*e.g.* SIBSON, 1975; ALLEN, 1979; MADDOCK, 1983; TOYOSHIMA, 1990). Mineral abbreviations are after KRETZ (1983).

3.1. Thermal peak of prograde metamorphism under non-deformational condition (D_1 stage)

The D_1 stage is defined by the formation of S_1 foliation parallel to lithologic boundaries and compositional layering (S_0) of the metamorphic rocks from Tonagh Island. There is generally very weak or no preferred orientation of minerals such as pyroxene on the S_1. Mineral lineation (L_1) on the S_1 foliation is scarcely recognizable. The L_1 lineation is different in orientation from post-D_1 lineations (Fig. 2).

A complex network of quartzofeldspathic veins cuts the D_1 structure and compositional layering (Fig. 3). Some of the veins intrude parallel to the S_1 and S_0.

Table 1. Tectonic and metamorphic history of ultrahigh-temperature metamorphic rocks from Tonagh Island. Tectonometamorphic episodes are from* SHERATON *et al. (1987).*

Deformation stage		Movement picture	Deformation & structure	Metamorphism	Tectono-metamorphic episode*
I	D_0	Formation of sedimentary precursors	?	Low-grade metamorphism ?	
	D_1	?	Non-deformational - very weakly deformationary conditions but partly flattening Bedding foliation (S_1) with no mineral lineation or very weak mineral lineation (L_1) or boudinage Quartzofeldspathic vein filling up fracture	Prograde metamorphism & anatexis? Metamorphic peak over 1000°C	D_1-M_1
II	D_2	Top-to-the ESE movement (dextral-reverse faulting) ?	Shearing & intrafolial folding NE-SW to E-W trending shear plane (foliation, S_2) with WNW-ESE trending mineral lineation (L_2) WNW-ESE trending fold with axial foliation	Initiation of retrograde metamorphism?	D_2-M_2
	D_3	Top-to-the ESE movement (dextral-reverse faulting)	Shearing, folding & retrograde mylonitization (High-temperature mylonitization) NE-SW trending mylonitic foliation (S_3) with strong mineral lineation (L_3) (thin mylonite) Mylonite, pseudotachylyte & foliated pseudotachylyte	Retrograde metamorphism granulite facies	
	D_4	E-W trending compression	N-S trending gentle folding		
III	D_5	N-S trending compression	WNW-ESE to E-W trending folding Tight to gentle fold with steep axial foliation (S_5) and minor shear zone	Retrograde metamorphism	D_3-M_3
	D_6	Top-to-the ESE, WNW, NE, NW, ESE or NW movements (sinistral-normal, reverse or dextral faulting)	Retrograde mylonitization & brittle deformation NE-SW to E-W trending mylonitic foliation with NW-SE to WNW-ESE trending mineral lineation Mylonite, pseudotachylyte & foliated pseudotachylyte NE-SW to E-W trending tight to gentle drag fold Intrusion of mafic dyke (metamorphosed & mylonitized)	Retrograde metamorphism granulite facies	
IV	D_7	Dextral faulting	N-S to NNE-SSW trending vertical joint with Grt-Hbl vein & minor mylonite zone	Retrograde metamorphism amphibolite facies	
	D_8	Sinistral faulting	NE-SW trending pseudotachylyte with N-S & NW-SE trending pseudotachylyte		
	D_9	?	Fracturing with pegmatite or dolerite dykes		

Some of the rocks undeformed after the D_1 stage are thin-layered gneisses that have well-developed lithologic boundaries and compositional layering (S_0). Therefore the S_0 may have been sedimentary precursors of the metamorphic rocks.

Boudins of layered gneiss with Grt-Opx assemblage and of coarse-grained Grt+Opx gneiss are found in quartzofeldspathic gneiss and in fine-grained Grt+Opx gneiss, respectively, with the S_1 foliation (Figs. 4A and B). The boudins range in length from a few tens of centimeters to several tens of meters and in thickness from several centimeters to fifteen meters (Figs. 4A and B). The D_1 boudins have a pancake shape, flattened parallel to the S_1 foliation and compositional layering. The shape of the boudins suggests that flattening type deformation occurred partly during the D_1 stage.

These D_1 structures have been preserved in some areas (*e.g.* a northeastern small peninsula) of the Island, though in the other areas post-D_1 deformations have modified most of the D_1 structures. Mineral assemblages such as Spr+Grt+Opx, Spl+Crn+Spr+Grt+Opx, Spl+Spr+Grt+Opx, Crn+Spl+Spr+Phl, Grt+Spr+Spl+Sil, Grt+Opx+Sil, Grt+Spr+Opx, Spr+Grt+Phl, Spr+Grt+Qtz and Opx+Sil+Qtz are often found in metamorphic rocks from the areas where the D_1 structures have been well preserved (*cf.* OSANAI *et al.*, 1995, 1999; HOKADA *et al.*, 1998). Therefore, the D_1 struc-

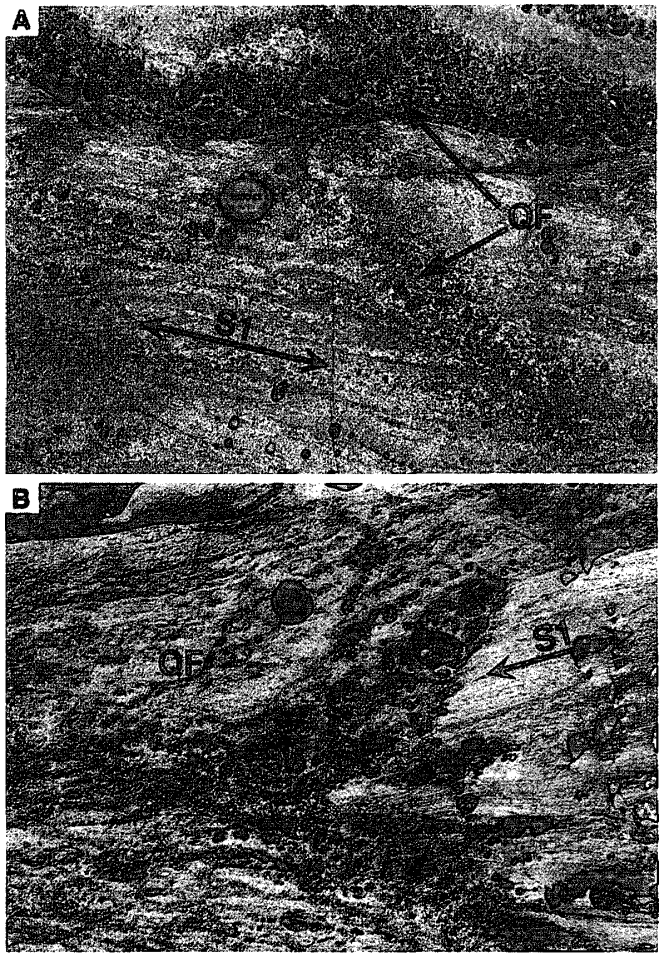

Fig. 3. *D_1 quartzofeldspathic vein (QF) cutting across S_1 foliation (S1) in the western part of unit II (A) and in the central part of unit I (B). S_1 is parallel to lithologic boundaries and compositional layering of sedimentary precursors of metamorphic rocks.*

ture would have been formed under non- or weakly-deformational condition during the thermal peak of prograde metamorphism.

3.2. Top-to-the-SE to -ESE displacement resulting in continuous layer-parallel shearing (D_2 stage)

The deformation of the D_2 stage is characterized by the formation of the NE-SW trending and NW dipping foliation (S_2) with the strong mineral lineation (L_2) (Figs. 1 and 2). The S_2 and L_2 structures are prominent ones in the Tonagh metamorphic rocks (Figs. 1 and 2) and are associated with asymmetrical rotated boudinage and asymmetrical intrafolial fold (B_2) with well-developed axial foliation (S_2') (Fig. 4C).

The S_2' axial foliation is parallel to subparallel to the S_2 foliation. The L_2 lineation is parallel to subparallel to the B_2 fold axis, dipping WNW. The S_2 and S_2' foliations and L_2 lineation are defined by orthopyroxene and related granulite facies mineral assemblages such as sapphirine (Fig. 4D). The D_1 quartzofeldspathic veins are rotated and elongated by the D_2 deformation, being parallel to the S_2 foliation in the rocks deformed strongly during the D_2 stage. Asymmetry of the D_2 structures shows the top-to-the-SE to

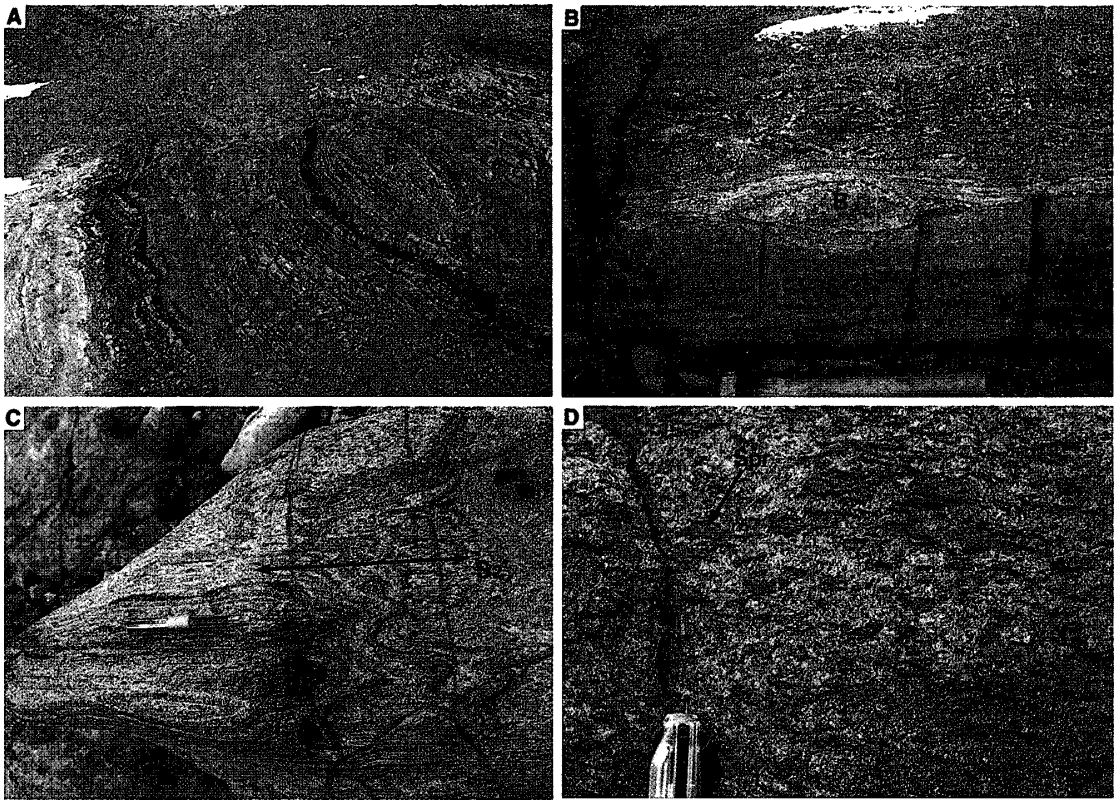

Fig. 4. D_1 and D_2 deformation structures. A: D_1 boudin (B) of Opx+Grt gneiss in orthopyroxene-bearing quartzofeldspathic gneiss from the eastern part of unit III. The boudin is about 5 meters in thickness. B: D_1 boudin (B) of coarse-grained Grt+Opx gneiss in fine-grained Opx+Grt gneiss from the eastern part of unit III. C: B_2 intrafolial fold with remarkable S_2' axial foliation in orthopyroxene-bearing quartzofeldspathic gneiss from the western part of unit II. D: L_2 mineral lineation defined by preferred dimensional orientation of elongated coarse sapphirine grains (Spr) in an intercalated Phl+Spr+Opx gneiss layer that is contained by orthopyroxene-bearing quartzofeldspathic gneiss from the southwestern part of unit IV.

-ESE movement (dextral-reverse shearing) of the Tonagh metamorphic rocks.

3.3. Thin shear zones resulting from top-to-the-SE to -ESE displacement (D_3 stage)

The D_3 stage is defined by the formation of thin shear zones parallel or oblique to S_2 foliation of surrounding gneiss (Figs. 1, 2 and 5). The width of the shear zones is between a few centimeters and a few tens of centimeters (Fig. 5). The D_3 shear zone consists mainly of anhydrous mylonite with pseudotachylyte, foliated pseudotachylyte and cataclasite (Fig. 5). The D_3 pseudotachylyte- and cataclasite-generating fault surfaces are parallel to S_2 foliation of the surrounding gneiss and to the S_2-parallel D_3 mylonite zone (Figs. 5C and D). Near the S_2-oblique D_3 mylonite zone, the S_2 foliation is curved toward the orientation parallel to the D_3 mylonite zone and its S_3 foliation (Fig. 5B). The mylonite and foliated pseudotachylyte show strong mylonitic foliation (S_3) with mineral lineation (L_3) (Figs. 1, 2 and 5). The S_3 foliation of the pseudotachylyte is continuous with and parallel to that of the D_3 mylonite. The D_3 pseudotachylyte veins cut the D_3 mylonitic structures of the D_3 mylonites and D_3 foliated pseudotachylytes. The S_3 folia-

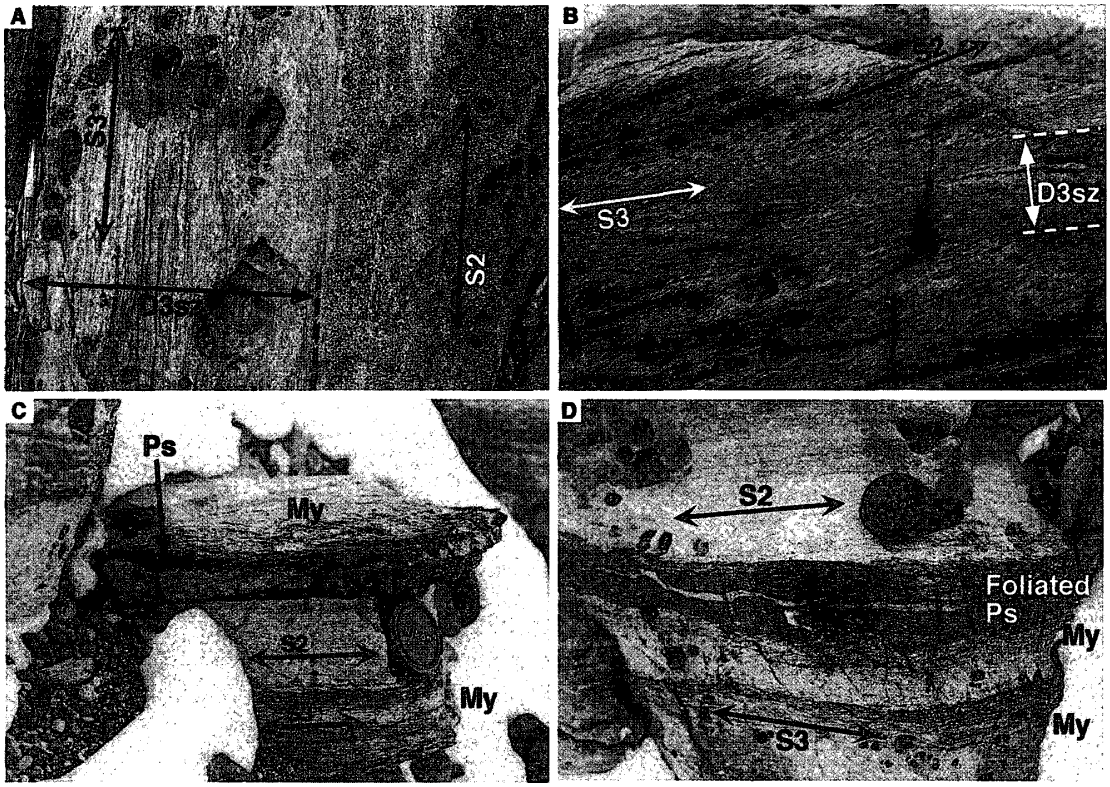

Fig. 5. D_3 shear zones. A: D_3 mylonite zone (D3sz) parallel to S_2 foliation (S2) in orthopyroxene-bearing quartzofeldspathic gneiss from the western part of unit II. The S_3 mylonitic foliation (S3) is parallel to the S_2 foliation. B: D_3 mylonite zone (D3sz) oblique to S_2 foliation (S2) in orthopyroxene-bearing quartzofeldspathic gneiss from the central part of unit II. The S_2 foliation is curved toward the orientation parallel to the D_3 mylonite zone and its S_3 foliation (S3). Top-to-the-SSE sense of shear. C: Thin D_3 mylonite zones (My) and D_3 pseudotachylyte vein (Ps) in garnet-bearing quartzofeldspathic gneiss from the northern part of unit V. The mylonite zones, S_3 mylonitic foliation (S3) and two pseudotachylyte-generating zones are parallel to S_2 foliation (S2) of the surrounding gneiss. D: D_3 foliated pseudotachylyte (Foliated Ps), which is parallel to D_3 mylonite zone (My) and S_2 foliation (S2), in garnet-bearing quartzofeldspathic gneiss from the northern part of unit V. The S_3 foliation (S3) of the pseudotachylyte is continuous with and parallel to that of the mylonite zone.

tion and L_3 lineation are defined by orthopyroxene, clinopyroxene and garnet, showing D_3 mylonitization during granulite facies conditions. Asymmetry of the D_3 mylonitic structures shows the top-to-the-SE to -ESE movement (*e.g.* Fig. 5B).

The D_3 cataclasite consists of a dark brown to brown cryptocrystalline matrix with numerous rock fragments and mineral fragments such as quartz, feldspar, garnet, sapphirine and orthopyroxene (Fig. 6A). Quartz and quartzofeldspathic fragments in the D_3 cataclasite rarely include sapphirine and garnet (Fig. 6). The sapphirine is commonly separated from quartz by reaction rims composed of one or more of sillimanite, garnet, orthopyroxene and alkali feldspar (Fig. 6B). A few grains of the sapphirine are in direct contact with quartz (Fig. 6A).

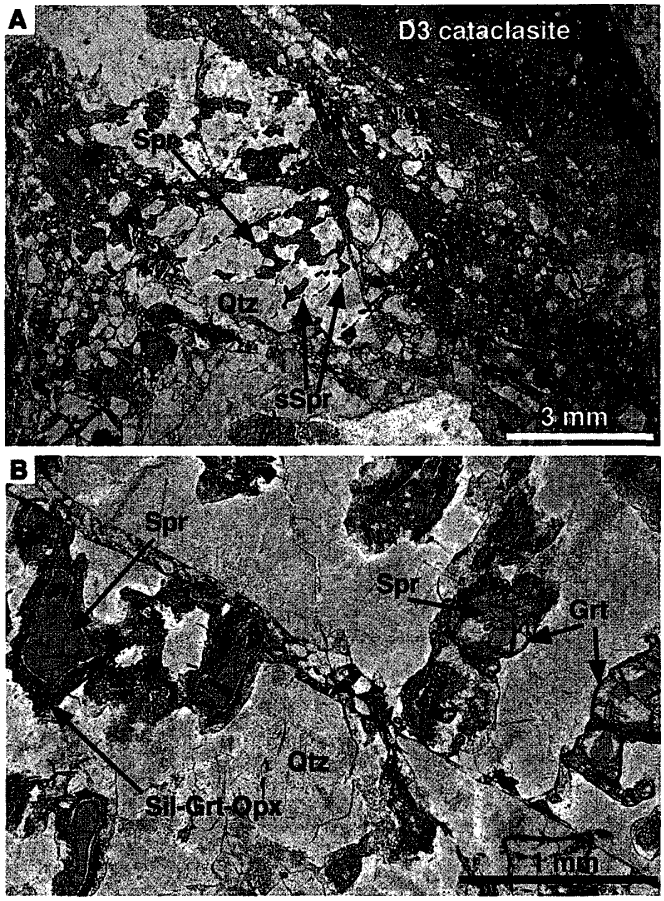

Fig. 6. Photomicrographs of D_3 cataclasite derived from garnet-, orthopyroxene- and sapphirine-bearing quartzofeldspathic gneiss in the western part of unit II. Plane-polarized light (PPL). A: D_3 cataclasite consisting of dark brown to brown cryptocrystalline matrix with numerous rock fragments and mineral fragments such as sapphirine (Spr)-including quartz (Qtz). A few small grains of the sapphirine (sSpr) are in contact with quartz. B: Quartz fragment (Qtz) which includes sapphirine (Spr) and garnet (Grt). The sapphirine grains are separated from quartz by reaction rims composed of one or more of garnet (Grt), sillimanite, orthopyroxene and alkali feldspar (Sill-Grt-Opx).

3.4. N-S trending folding resulting from E-W compression (D_4 stage)

The D_4 stage is defined by the formation of N-S trending folds (B_4) of pre-D_4 structures. The D_4 folds form open to gentle shapes with subhorizontal fold axis and subvertical axial plane (Figs. 1 and 7). The B_4 folds, which are geological-map scale antiforms and synforms, are found in the southern part of Tonagh Island and have been refolded by post-D_4 folding (Figs. 1 and 7). The D_4 folding may have been attributed to E-W compression.

3.5. N-S trending compression resulting in WNW-ESE to E-W trending folds (D_5 stage)

The deformation of the D_5 stage is characterized by WNW-ESE to E-W trending folds (B_5) of pre-D_5 structures and by refolding of pre-D_5 folds such as the B_2 and B_4 folds (Figs. 1, 2 and 7). The B_5 folds form tight to gentle shapes with subvertical to steep axial foliation (S_5) that is inclined to the pre-existing foliation (Fig. 7). The S_5

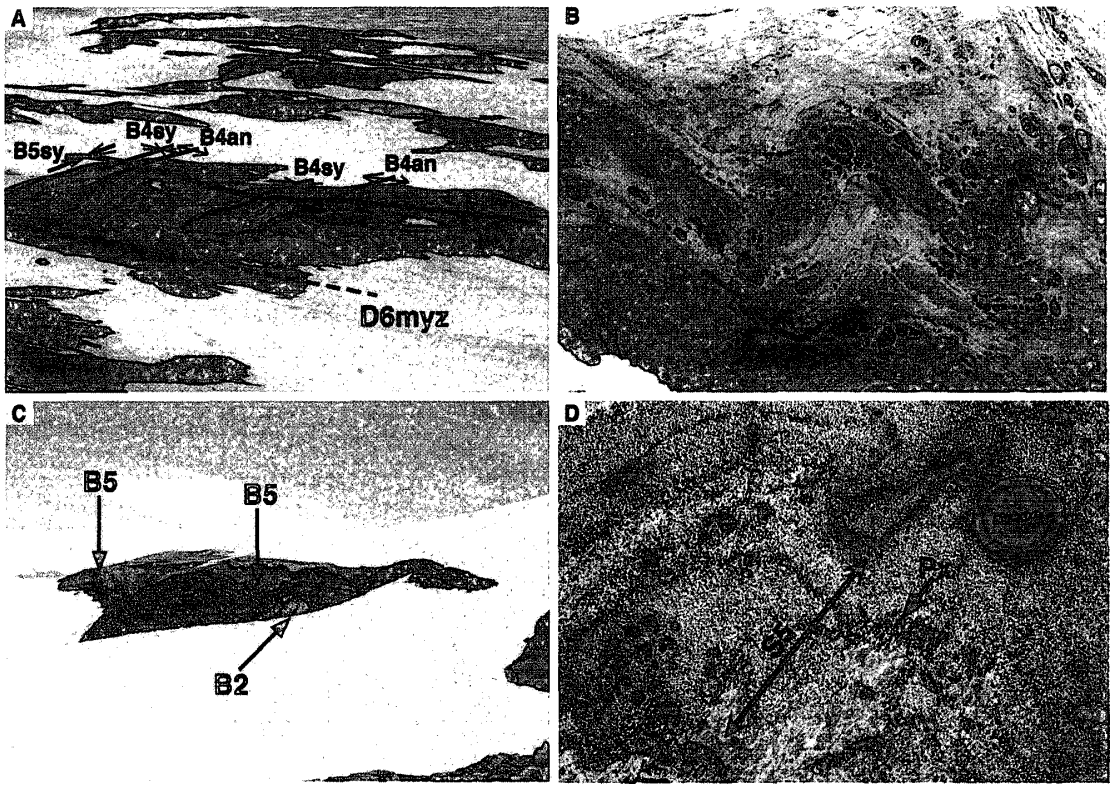

Fig. 7. *B_4 and B_5 folds. A: B_4 antiforms (B4an) and B_4 synforms (B4sy) refolded by the B_5 synform (B5sy) in the northern part of unit V. The B_5 fold is cut by the D_6 mylonite zone (D6myz) in unit V. The central part of the photograph is approximately 600 meters wide. B: B_5 fold with close to open shape in orthopyroxene-bearing quartzofeldspathic gneiss from the northern part of unit V. The lens cap of the camera is 5.2 centimeters in diameter. C: B_5 fold (B5) refolding B_2 intrafolial fold (B2) of layered gneiss at the eastern end of unit IV. The cliff height is about 40 meters. D: B_5 fold of layered gneiss with remarkable S_5 axial foliation (S5) at the western end of unit IV. The S_5 foliation is defined by preferred dimensional orientation of elongated coarse orthopyroxene and clinopyroxene grains (Px).*

foliation is defined by orthopyroxene and related granulite facies assemblages (Fig. 7D). Some of the folds are geological-map scale antiforms and synforms (Figs. 1 and 7A). The geological-map scale D_5 folds are developed in the eastern and western parts of the island. Their fold axes plunge gently westward. The folds with small interlimb angles are associated with minor shear zones at their fold limbs. The D_5 folding may have been due to N-S compression.

3.6. Formation of unit boundary fault associated with mylonitization and seismic faulting (D_6 stage)

The deformation of the D_6 stage is characterized by the formation of NE-SW to E-W trending and steeply NW to N dipping thick mylonite zones, accompanied by drag folds (B_6) (Figs. 1, 2 and 8). Most of the D_6 mylonite zones occur along the unit boundary faults between lithologic units (Fig. 1). A D_6 mylonite zone also occurs in unit IV (Fig. 1). The D_6 mylonite zones cut pre-D_6 structures such as the S_2 foliation and B_5 fold (Figs. 7A and 8C), and consist of anhydrous mylonite with pseudotachylyte and foliated

pseudotachylyte (Figs. 8A, 9 and 10). The D_6 mylonites and D_6 foliated pseudotachylytes show strong mylonitic foliation (S_6) and mineral lineation (L_6) (Figs. 1, 2 and 8A). The pre-D_6 foliations of gneisses near the D_6 mylonite zones are curved toward the orientation parallel to the D_6 mylonite zone and its S_6 foliation (Fig. 1). The L_6 lineations are parallel, oblique or perpendicular to the dip of the S_6 foliation. The D_6 mylonite zones may have resulted from poly-phase deformation.

The S_6 foliation and L_6 lineation of the D_6 mylonites are defined by the preferred dimensional orientations of elongated porphyroclasts and recrystallized fine-grained anhydrous minerals. The porphyroclastic minerals in the D_6 mylonite are garnet, orthopyroxene, clinopyroxene and alkali feldspar (Fig. 9). The recrystallized matrix minerals of the mylonite are mainly quartz, feldspars, orthopyroxene, clinopyroxene and garnet (Fig. 9). Garnet and orthopyroxene porphyroclasts are associated with asymmetrical tails of recrystallized fine-grained garnet and orthopyroxene, respectively (Fig. 9A). Alignment of the long axes of dynamically recrystallized fine-grained orthopyroxenes

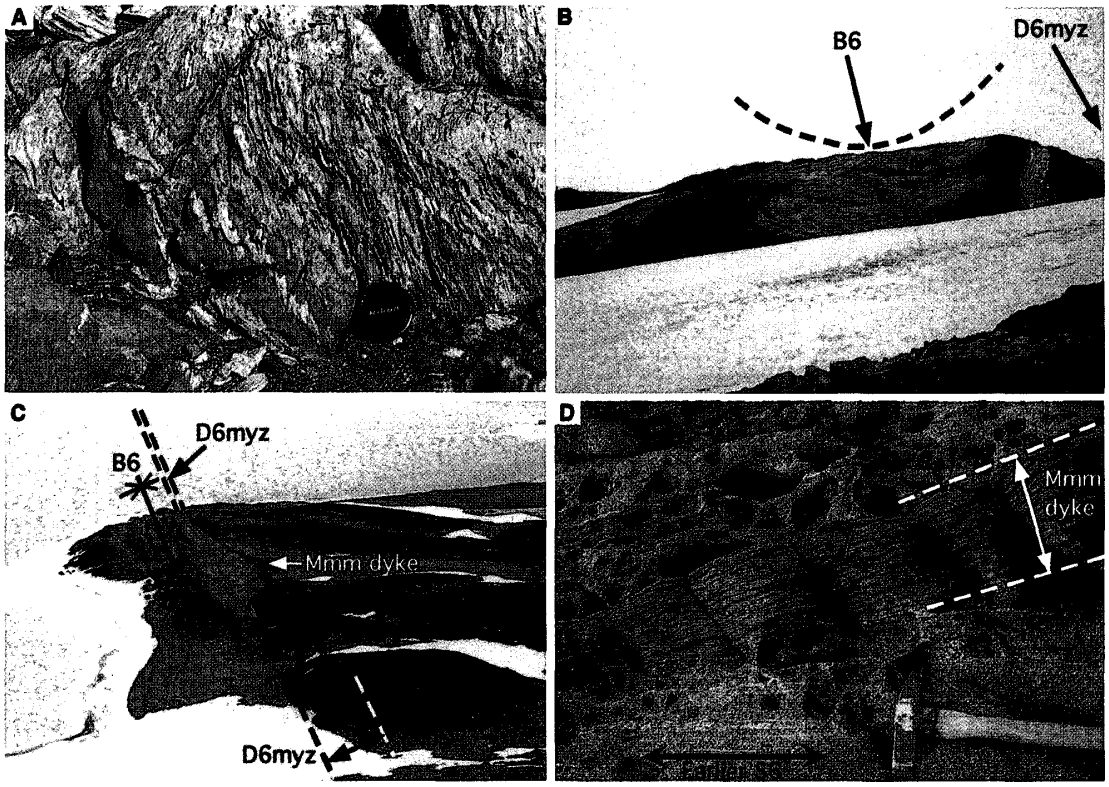

Fig. 8. D_6 mylonite zone and related deformation structures. A: Extremely foliated and folded rocks in the D_6 mylonite zone along the eastern part of the boundary fault between units II and III. B: Gentle drag fold (synform) (B6) accompanying the D_6 mylonite zone (D6myz) along the eastern part of the boundary fault between units II and III. The central part of the photograph is about 80 meters across. C: D_6 mylonite zone (D6myz) accompanied by drag fold (synform) (B6) and a metamorphosed and mylonitized mafic dyke (Mmm dyke) along the western part of the boundary fault between units II and III. The D_6 mylonite zone is approximately 60 meters in maximum thickness. D: Mafic dyke (Mmm dyke) intruding into the thickest D_6 mylonite zone along the boundary fault between units II and III. The dyke cuts S_6 formed during the earlier D_6 stage (Earlier S6), and then was mylonitized and metamorphosed during the later D_6 stage.

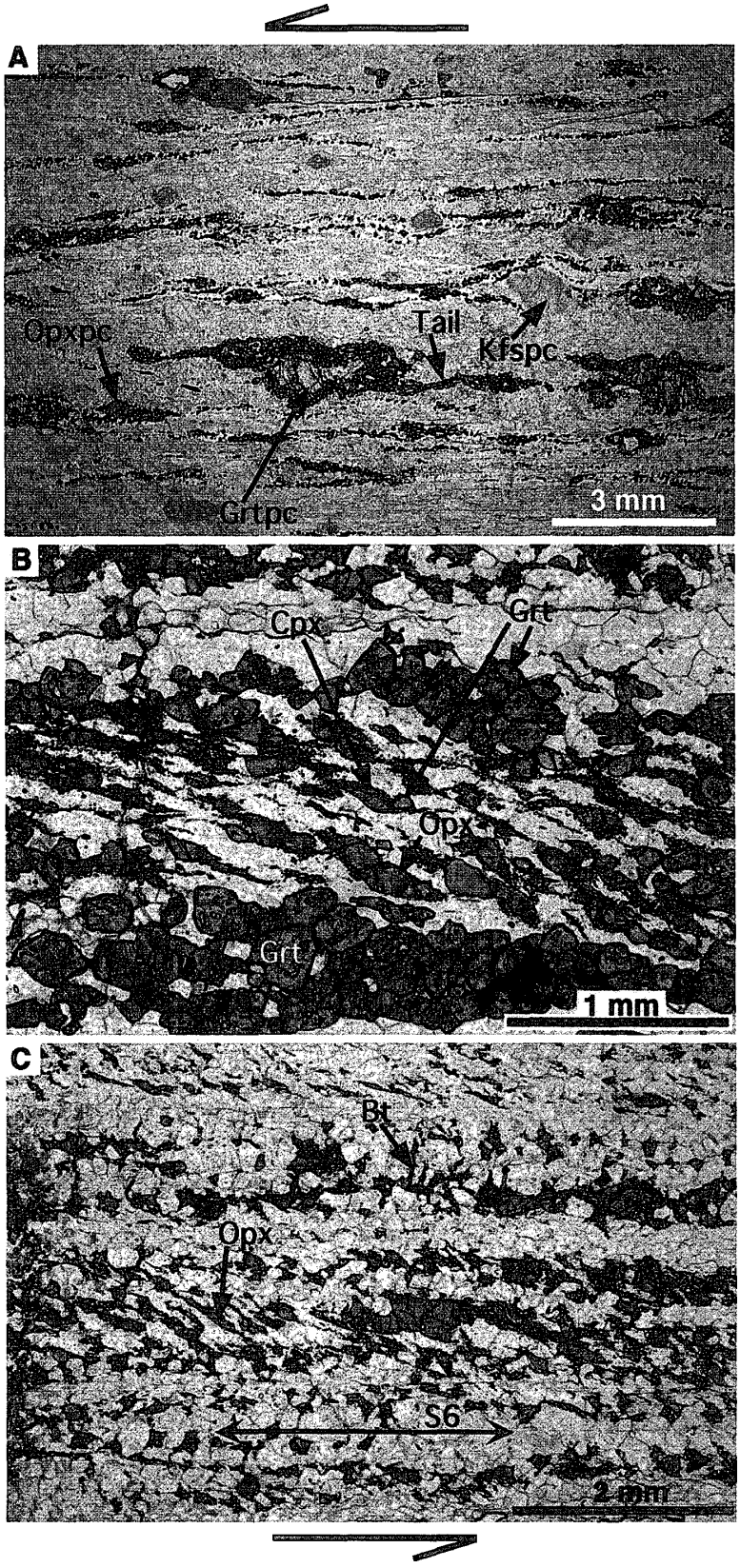

Fig. 9. Photomicrographs of D_6 mylonites. PPL. A: D_6 mylonite derived from garnet- and orthopyroxene-bearing quartzofeldspathic gneiss along the eastern part of the boundary fault between units II and III. The porphyroclastic minerals in the mylonite are garnet (Grtpc), orthopyroxene (Opxpc) and alkali feldspar (Kfspc). The matrix minerals of the mylonite are mainly quartz, feldspar, orthopyroxene and garnet. Garnet (Grtpc) and orthopyroxene porphyroclasts are associated with asymmetrical tails of recrystallized fine-grained garnet (Tail) and orthopyroxene, respectively. Top-to-the-SE (dextral-reverse) sense of shear. B: D_6 Opx-Cpx-Grt mylonite formed along the western part of the boundary fault between units II and III. Alignment of the long axes of dynamically recrystallized fine grains of orthopyroxene (Opx), clinopyroxene (Cpx) and garnet (Grt) define oblique grain shape fabrics. Top-to-the-W (sinistral-normal) sense of shear. C: Random-oriented biotite grains (Bt) cutting S_6 mylonitic foliation (S6) in D_6 mylonite along the western part of the boundary fault between units II and III. Oblique grain shape fabrics of dynamically recrystallized fine-grained orthopyroxene grains (Opx) indicate top-to-the-W (sinistral-normal) sense of shear.

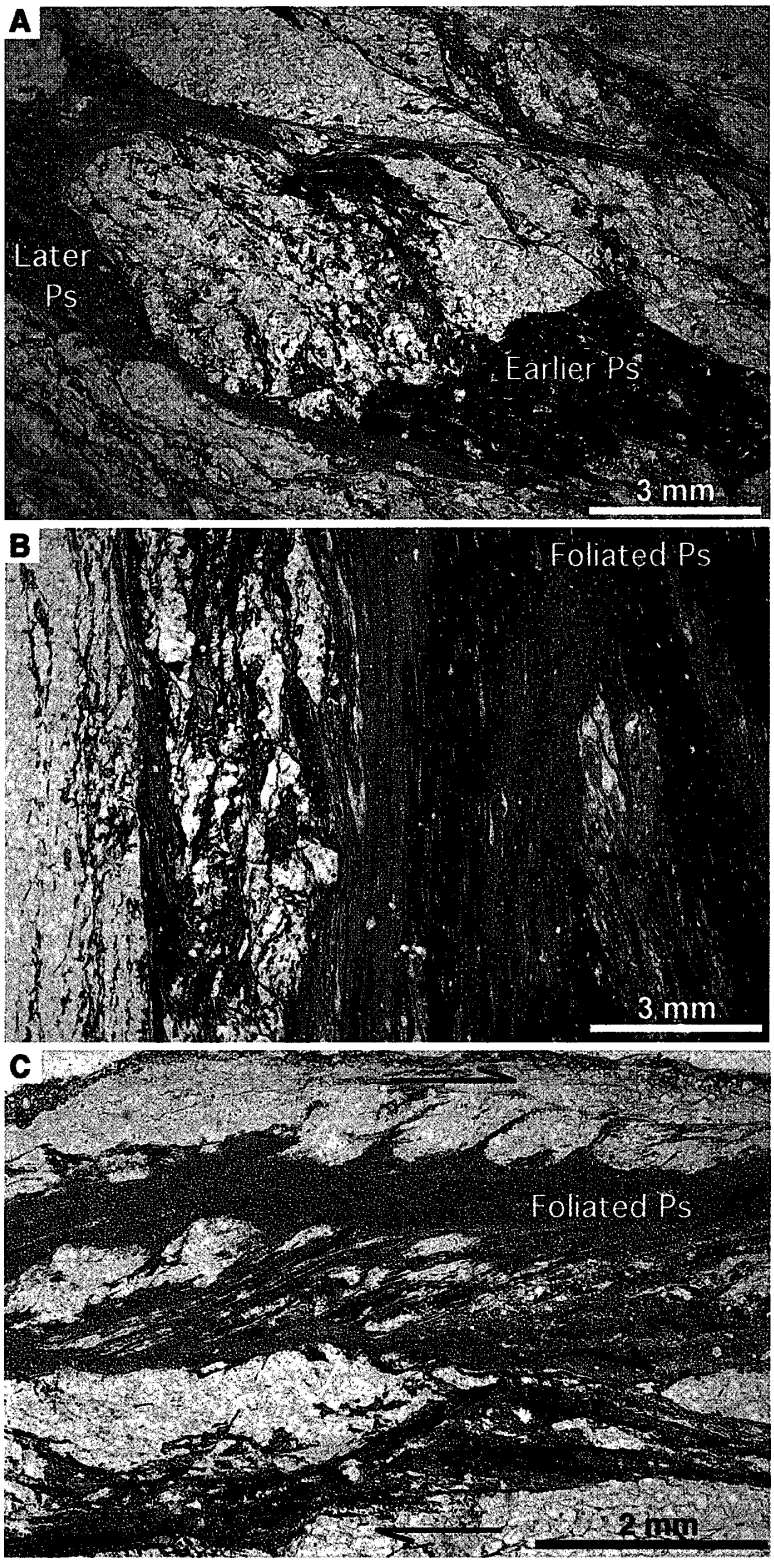

Fig. 10. D_6 pseudotachylyte (Ps) and foliated pseudotachylyte (Foliated Ps). PPL. A: Later D_6 pseudotachylyte (Later Ps) cutting earlier D_6 pseudotachylyte (Earlier Ps) in the D_6 mylonite zone along the western part of the boundary fault between units II and III. B: D_6 foliated pseudotachylyte in the D_6 mylonite zone along the western part of the boundary fault between units II and III. The S_6 foliation of the pseudotachylyte is continuous with and parallel to that of the surrounding D_6 mylonite. C: ditto. Asymmetry of quartzofeldspathic boudin and mylonitic foliation indicates top-to-the-SE (reverse) sense of shear.

and/or garnets define oblique grain-shape fabrics. Most of the asymmetrical structures and textures indicate a top-to-the-NW to -W (sinistral-normal to sinistral) sense of shear (Figs. 9B and C). Some of them show a top-to-the-SE to -ESE (reverse to dextral-reverse) sense of shear (Fig. 10A). Shear indicators in the top-to-the-W sense are mainly found in finer-grained mylonites (highly strained zones) with gently plunging L_6 lineations in the D_6 mylonite zone. A few of the D_6 mylonites with subhorizontal L_6 lineation show a top-to-the-ENE to -E (dextral) sense of shear. The subhorizontal lineation cuts the steeply plunging L_6 lineations.

Random-oriented and non-deformed biotite grains cut the S_6 mylonitic structures (Fig. 9C). Grain coarsening of quartz is often recognizable in the dynamically recrystallized fine-grained matrix of the D_6 mylonites. The new coarse quartz grains show slight undulatory extinction, suggesting almost strain-free conditions. Also, asymmetrical structures such as S, C and C' surfaces are present but only faintly visible in the D_6 mylonites (Figs. 9A and C). These appear to have been due to hydration, reheating or annealing under almost non-deformational conditions after the D_6 deformation (*cf.* BARKER, 1998).

Most of the D_6 foliated pseudotachylytes show more remarkable S_6 foliation than the D_6 mylonites and occur as ultramylonite layers parallel to the S_6 foliation in the D_6 mylonite zones. Some of the D_6 foliated pseudotachylytes show weak D_6 structures and characteristically branch into blind-ending veins (injection veins), showing intrusive relations to the surrounding D_6 mylonites. The weakly foliated pseudotachylytes also include fragments of strongly foliated mylonites. The S_6 foliations of both strongly- and weakly-foliated pseudotachylytes are continuous with, and parallel to subparallel to, that of the surrounding D_6 mylonite and to the trend of the D_6 mylonite zone. The S_6 mylonitic foliation of the weakly foliated pseudotachylyte cuts across the boundaries between the mylonites and injection veins. These show that pseudotachylyte has been formed after earlier D_6 mylonitization and then subjected to later D_6 mylonitization, resulting in the formation of the foliated pseudotachylyte during the later D_6 stage.

The S_6 foliation and L_6 lineation of the foliated pseudotachylytes are defined by elongated rock and mineral fragments and by alignment of fine-grained minerals of the matrix (Figs. 10B and C). Quartz and feldspar are commonly recognizable as mineral fragments under the microscope, but fragments of mafic minerals such as pyroxenes and garnet are extremely rare. The fragments of quartz, feldspars and quartzofeldspathic rocks are mylonitized. The fine-grained matrix minerals of the foliated pseudotachylytes are mainly quartz, feldspar, biotite, garnet and orthopyroxene. Random-oriented and non-deformed biotite grains are found in weakly deformed parts of the matrix in the foliated pseudotachylyte and in the surrounding mylonites. These indicate that the formation of the pseudotachylytes and their mylonitization during the later D_6 stage took place under granulite facies conditions.

Asymmetry of quartzofeldspathic boudins and mylonitic structures indicates a top-to-the-SE (reverse) sense of shear during the later D_6 mylonitization (Figs. 10B and C).

The D_6 pseudotachylytes occur as simple veins, fault veins and injection veins, a ladder network of veins and quasi-conglomerate with pseudotachylyte matrix (SIBSON, 1975). Each vein is not more than several centimeters thick. Most of the veins characteristically branch into narrow irregular veins, showing marked intrusive relations to the

host rocks. The D_6 pseudotachylyte-generating fault surfaces (fault veins) are parallel to subparallel to the trend of the D_6 mylonite zone and to S_6 foliation of the surrounding D_6 mylonite. The fault veins and injection veins form asymmetrical network patterns. The asymmetry and separation along those veins indicate a top-to-the-NW (normal) sense of shear.

The D_6 pseudotachylyte consists of a black or dark brown cryptocrystalline matrix with numerous rock fragments and mineral fragments such as quartz and/or feldspar. The rock and mineral fragments are randomly oriented and are considered from lithological similarity to be derived from the surrounding host mylonite. Quartz and feldspars are commonly recognizable as mineral fragments under the microscope, but fragments of mafic minerals such as pyroxenes and garnet are extremely rare. Pseudotachylyte veins that sharply cut other veins and foliated pseudotachylytes can also be found (Fig. 10A). This indicates multiphase formation of pseudotachylyte, i.e., repeated seismic faulting, after the later D_6 mylonitization.

The B_6 drag folds, which develop near and in the D_6 mylonite zones (unit boundary faults), form isoclinal to gentle shapes with subvertical axial foliation (S_6'). Many folds are of asymmetric type; some folds show rootless forms, owing to a high-strain magnitude during the D_6 folding. Some of the B_6 folds are geological-map scale antiforms and synforms (Fig. 1).

Field observation and structural relations of fault rocks as mentioned above suggest mylonite, pseudotachylyte, foliated pseudotachylyte and associated mylonite, and pseudotachylyte were formed in turn during the D_6 stage. The earlier D_6 mylonites have been formed through reverse to dextral-reverse, sinistral-normal to sinistral, and dextral layer-parallel shearing. Earlier D_6 pseudotachylyte veins cut the earlier D_6 mylonitic structures, and then were mylonitized and foliated by the top-to-the-SE (reverse) sense of shearing in the later D_6 stage. Subsequently, seismic faulting of the latest D_6 stage took place along the D_6 mylonite zones and the later pseudotachylytes resulted from the top-to-the-NW (normal) sense of shearing. Mafic dykes intruded into the thickest mylonite zone, cutting earlier S_6 foliation, and then were mylonitized and metamorphosed during the later D_6 stage (Figs. 8C and D).

3.7. Dextral faulting associated with Grt+Hbl veining (D_7 stage)

The N-S to NNE-SSW trending vertical faults (F_7) and joints (J_7) cut pre-D_7 structures (Figs. 11A and B). The D_7 brittle structures are associated with Grt+Hbl veins and thin mylonite zones consisting of Grt+Hbl+Pl (Figs. 11A and B). This indicates that D_7 deformation was associated with hydration and occurred under retrograde amphibolite facies conditions. Asymmetry of the D_7 structures shows that dextral faulting occurred during the D_7 stage (Figs. 11A and B).

3.8. Sinistral seismic faulting resulting in frictional melting (D_8 stage)

The D_8 stage deformation is characterized by NE-SW trending pseudotachylyte zones with N-S and WNW-ESE trending pseudotachylyte zones (Figs. 11C and D). The latter two zones were formed by secondary shearing of the former zone, showing that sinistral seismic faulting took place during the D_8 stage.

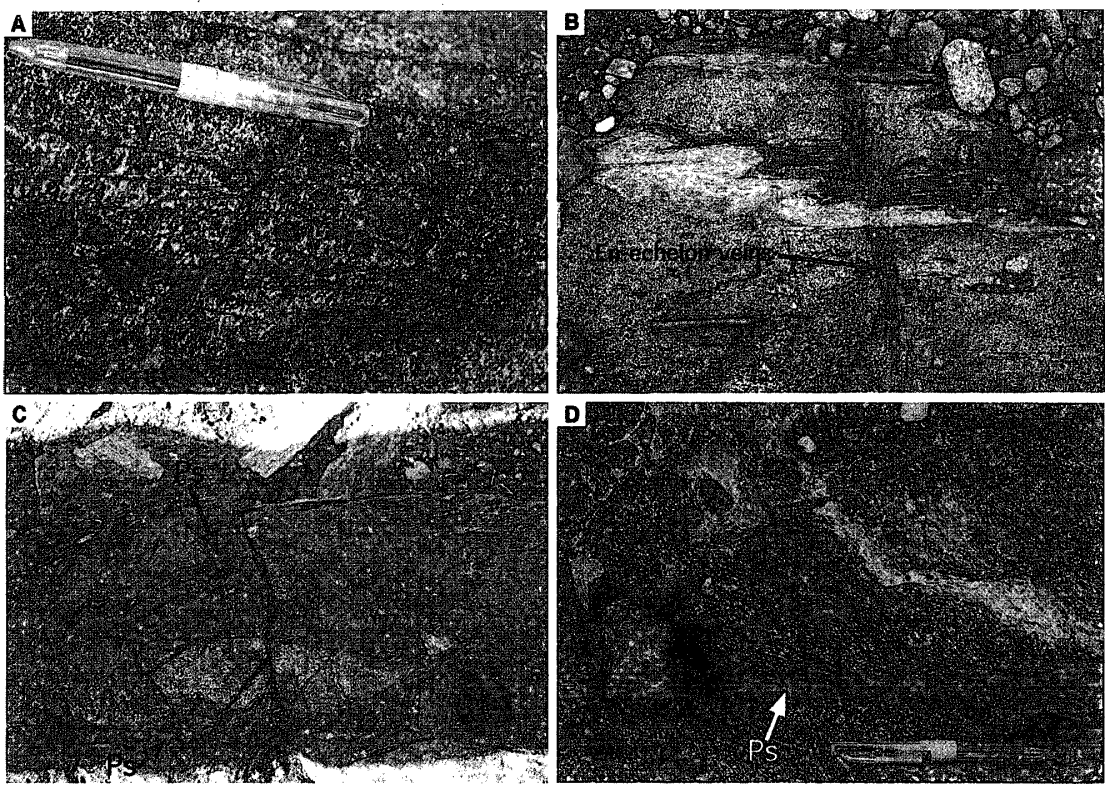

Fig. 11. D_7 veins and D_8 pseudotachylyte (Ps) found in the western part of unit II. A: Grt-Hbl veins (arrows). B: D_7 en-echelon veins indicating dextral sense of shear. C: Thick WNW-ESE trending D_8 pseudotachylyte zone. D: Thin NE-SW trending D_8 pseudotachylyte vein. The S_2 foliation of the surrounding mafic gneiss is curved toward the orientation parallel to the vein, showing a sinistral sense of shear.

3.9. Pegmatite and dolerite intrusions (D_9 stage)

The D_9 stage deformation is defined by the formations of pegmatite and dolerite dykes cutting across pre-D_9 structures (Fig. 1). After the D_9 stage, no deformation took place on Tonagh Island. The movements during the pegmatite and dolerite intrusions are still unknown.

4. Concluding Remarks

The deformation history of ultrahigh-temperature metamorphic rocks from Tonagh Island is divided into nine stages, from D_1 to D_9, based on the characteristics of deformation structures, deformation textures and movement pictures (Table 1 and Fig. 12), as mentioned in the previous section. The D_1 structure would have been formed under a non-deformational condition during the thermal peak of prograde metamorphism. Many metamorphic belts have been detached and exhumed associated with mylonitization, retrograde metamorphism and magmatic intrusion after their thermal peaks of prograde metamorphism (*cf.* FOUNTAIN *et al.*, 1992; PRECIVAL *et al.*, 1992; RUTTER *et al.*, 1993; TOYOSHIMA *et al.*, 1994, 1996). Therefore, deformations during the D_2–D_6 stages would have occurred under retrograde granulite facies conditions during the detachment and exhumation of the UHT rocks of Tonagh Island from deep crustal levels (*cf.* TSUNOGAE

et al., 1998, 1999; HOKADA *et al.*, 1998). However, a large amount of magmatic intrusion related to the detachment and exhumation of the UHT rocks is not recognizable, in contrast to other metamorphic belts. The D_1 quartzofeldspathic intrusions may have been related to the initial stage of the exhumation tectonics of the UHT rocks from Tonagh Island.

During the D_2 stage, most of the UHT rocks from Tonagh Island have suffered continuous layer-parallel shearing resulting from the top-to-the-SE to -ESE displacement (Fig. 12). The subsequent D_3 shearing is the same in shear sense as the previous D_2 stage (Fig. 12). Therefore, it can be considered that as the deformation progressed from the D_2 to D_3 stages, the mylonitization due to shearing in the top-to-the-SE to -ESE sense was locally concentrated in D3 narrow shear zones.

After the D_4 E-W compression and the D_5 N-S trending compression, unit boundary faulting took place associated with the D_6 mylonite zones (Fig. 12). The D_6 mylonite zones appear to be formed through multiphase deformation during the D_6 stage as

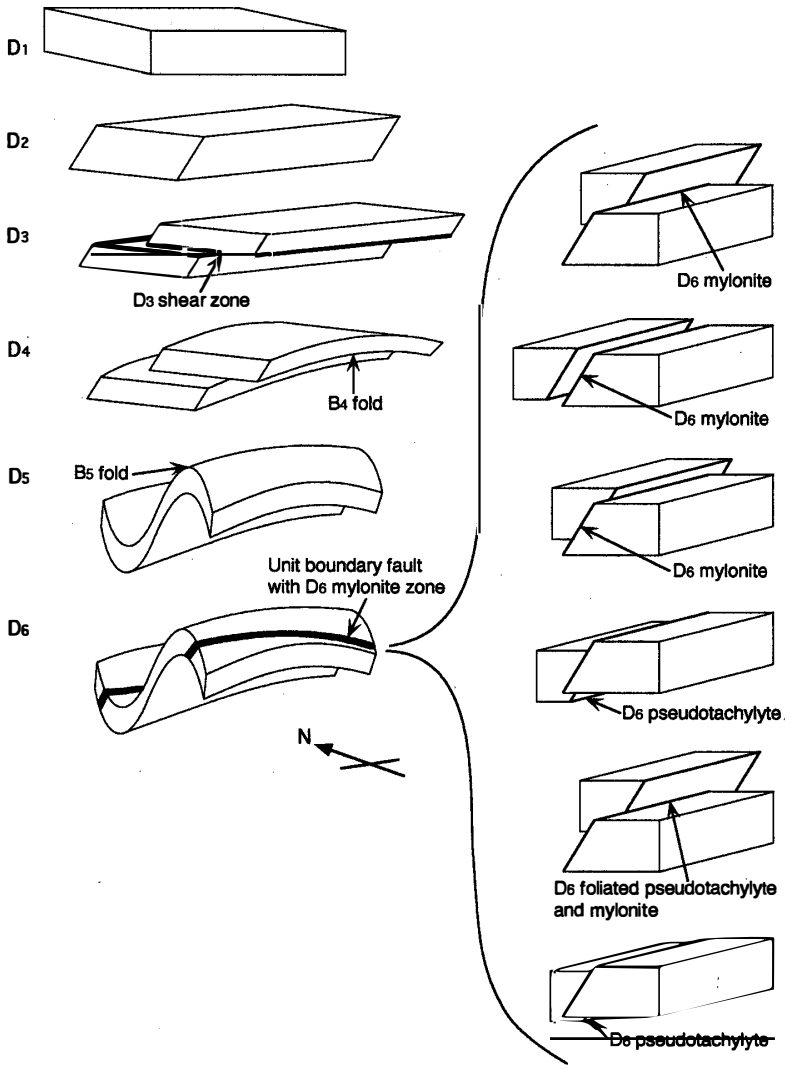

Fig. 12. Schematic diagram illustrating the structural evolution of ultrahigh-temperature metamorphic rocks from Tonagh Island that occurred during the D_1 to D_6 stages.

follows. During the earlier D_6 stage, the top-to-the-SE (reverse to dextral-reverse) shearing, the top-to-the-NW to -W (sinistral-normal to sinistral) shearing with highly strained zones and then the top-to-the-ENE to -E (dextral) shearing occurred. The earlier D_6 seismic faulting followed the earlier D_6 mylonitization, and was followed by later D_6 mylonitization due to the top-to-the-SE (reverse) shearing. Subsequently the seismic faulting of the latest D_6 stage would have taken place due to brittle shearing in the top-to-the-NW (normal) sense. The deformation history during the D_6 stage still remains unsolved.

The earlier D_3 pseudotachylyte veins cut the earlier D_3 mylonitic structures and then were mylonitized and foliated during the later D_3 stage. The earlier D_6 pseudotachylyte veins cut the earlier D_6 mylonitic structures and then were mylonitized and foliated during the later D_6 stage. The later D_3 and later D_6 pseudotachylytes cut the D_3 and D_6 foliated pseudotachylytes, respectively. These suggest that seismic faulting and plastic deformation (mylonitization) alternated under retrograde granulite facies conditions during the D_3 and D_6 stages.

The tectonic and metamorphic history of the UHT metamorphic rocks from Tonagh Island is largely divided into three stages (I, II and III) based on the nature and characteristics of deformation and metamorphism (Table 1). Stage I (D_0 and D_1) is of prograde metamorphism and its thermal peak. During the subsequent stage II (D_2 to D_4), ductile deformation or seismic faulting occurred under retrograde granulite facies conditions. The following stage III deformations (D_5 and D_6) resulted in the formation of the unit boundary faults and related structures. During the subsequent stage IV (D_7 to D_9), brittle deformations took place under retrograde amphibolite facies conditions or lower, and modified in part the exhumed metamorphic rocks of Tonagh Island.

In the above described deformation history of the UHT rocks from Tonagh Island, the Amundsen dolerite dyke is the product of the last stage (D_9). Therefore, the deformation from the D_1 to D_8 stages mentioned above corresponds to first to third tectonometamorphic episodes of the whole Napier Complex (Table 1) (JAMES and BLACK, 1981; SHERATON *et al.*, 1987; BLACK, 1988; HARLEY and HENSEN, 1990). The D_1 stage of the UHT rocks may have been correlated with the first episode (D_1–M_1) during the thermal peak of the prograde metamorphism (Table 1) (*e.g.* SHERATON *et al.*, 1987). The D_5 to D_6 stages would be correlated with the third tectonometamorphic episode (D_3–M_3), based on orientation of the fold axis and axial plane, attitude and tightness of fold and geometry of fold profile (Table 1) (SHERATON *et al.*, 1987; HARLEY, 1987). The regional strike in most of the Napier Complex is largely the result of the third deformation episode (D_3–M_3) which occurred during the waning stages of the high-grade metamorphism (*e.g.* SHERATON *et al.*, 1987). Though the S_2 foliation and L_2 lineation are prominent in the UHT rocks from Tonagh Island, most of these structures were highly folded and faulted during the D_5 to D_6 stages. This also suggests that the third tectonometamorphic episode of the whole Napier Complex corresponds to the D_5 to D_6 stages in the deformation history of the UHT rocks from Tonagh Island (Table 1). Hydration, reheating or annealing of the UHT rocks would have occurred under almost non-deformational conditions after the D_6 deformation, as shown by the difficulty in recognizing mylonitic structures of the D_6 mylonites.

Acknowledgments

We are grateful to members of JARE-39 and -38 and the crew of the icebreaker SHIRASE for their support during the 1997–1998 season. Drs. H. ISHIZUKA, M. ISHIKAWA, K. SHIRAISHI, and Y. MOTOYOSHI and Ms. S. SUZUKI are acknowledged for their invaluable discussions and helpful advice.

References

ALLEN, A.R. (1979): Mechanism of frictional fusion in fault zones. J. Struct. Geol., **1**, 231–243.

ASAMI, M., SUZUKI, K., GREW, E.S. and ADACHI, M. (1998): CHIME ages for granulites from the Napier Complex, East Antarctica. Polar Geosci., **11**, 172–199.

BARKER, A.J. (1998): Introduction to Metamorphic Textures and Microstructures. 2nd ed. Cheltenham, Stanley Thornes Publ., 264 p.

BLACK, L.P. (1988): Isotopic resetting of U-Pb zircon and Rb-Sr and Sm-Nd whole-rock systems in Enderby Land, Antarctica: Implication for the interpretation of isotopic data from polymetamorphic and multiply deformed terrains. Precambrian Res., **38**, 355–365.

FOUNTAIN, D.M., ARCULUS, R. and KAY, R.W., ed. (1992): Continental Lower Crust. Netherlands, Elsevier, 485 p. (Developments in Geotectonics, **23**).

HARLEY, S.L. (1987): A pyroxene-bearing meta-ironstone and other pyroxene-granulites from Tonagh Island, Enderby Land, Antarctica: Further evidence for very high temperature (>980°C) Archaean regional metamorphism in the Napier Complex. J. Metamorph. Geol., **5**, 341–356.

HARLEY, S.L. (1998): On the occurrence and characterization of ultrahigh-temperature crustal metamorphism. What Drives Metamorphism and Metamorphic Reactions? ed. by P.J. TRELOAR and P.J. O'BRIEN. London, Geol. Soc., 81–107 (Geol. Soc. London, Spec. Pub., **138**).

HARLEY, S.L. and HENSEN, B.J. (1990): Archaean and Proterozoic high-grade terranes of East Antarctica. (40–80°E): A case study of diversity in granulite facies metamorphism. High-temperature Metamorphism and Crustal Anatexis. ed. by J. R. ASHWORTH and M. BROWN. London, Unwin Hyman, 320–370 (Mineral. Soc. Ser., **2**).

HOKADA, T., OSANAI, Y., TOYOSHIMA, T., OWADA, M., TSUNOGAE, T. and CROWE, W.A. (1998): UHT metamorphism of aluminous gneisses from Tonagh Island in the Napier Complex, Enderby Land. The 18th Symposium on Antarctic Geosciences, Program and Abstracts, 20–21 October 1998. Tokyo, Natl Inst. Polar Res., 31–32.

JAMES, P.R. and BLACK, L.P. (1981): A review of the structural evolution and geochronology of the Archaean Napier Complex of Enderby Land, Australian Antarctic Territory. Archaean Geology: Second International Symposium, Perth, 1980, ed. by J.E. GLOVER and D.I. GROVES. Sydney, Geol. Soc. Aust., 71–83 (Spec. Publ. Geol. Soc. Aust., **7**).

KRETZ, R. (1983): Symbols for rock-forming minerals. Am. Mineral., **68**, 277–279.

MADDOCK, R.H. (1983): Melt origin of fault-generated pseudotachylytes demonstrated by textures. Geology, **11**, 105–108.

OSANAI, Y., OWADA, M., SHIRAISHI, K., HENSEN, B.J. and TSUCHIYA, N. (1995): Ultrahigh-temperature dehydration melting of F-biotite in pelitic granulites from the Napier Complex, Enderby Land, East Antarctica. The 15th Symposium on Antarctic Geosciences, Program and Abstract, October 1995. Tokyo, Natl Inst. Polar Res., 79 (in Japanese).

OSANAI, Y., TOYOSHIMA, T., OWADA, M., TSUNOGAE, T., HOKADA, T. and CROWE, W.A. (1998): Geology and protolith of ultrahigh-temperature metamorphic rocks from Tonagh Island in the Napier Complex, East Antarctica. The 18th Symposium on Antarctic Geosciences, Program and Abstract, 20–21 October 1998. Tokyo, Natl Inst. Polar Res., 25–26 (in Japanese).

OSANAI, Y., TOYOSHIMA, T., OWADA, M., TSUNOGAE, T., HOKADA, T. and CROWE, W.A., (1999): Geology of ultrahigh-temperature metamorphic rocks from Tonagh Island in the Napier Complex, East Antarctica. Polar Geosci., **12**, 1–28.

OWADA, M., OSANAI, Y. and KAGAMI, H. (1994): Isotopic equilibration age of Sm-Nd whole-rock system in the

Napier Complex (Tonagh Island), East Antarctica. Proc. NIPR Symp. Antarct. Geosci., **7**, 122–132.

OWADA, M., OSANAI, Y., HAMAMOTO, T. and KAGAMI, H. (1996): Sm-Nd garnet-whole rock isochron age from Tonagh Island, Napier Complex. The 16th Symposium on Antarctic Geosciences, Program and Abstract, October 1996. Tokyo, Natl Inst. Polar Res., 42–43 (in Japanese).

PRECIVAL, J.A., FOUNTAIN, D.M. and SALISBURY, M.H. (1992): Chapter 8. Exposed crustal cross sections as windows on the lower crust. Continental Lower Crust, ed. by D.M. FOUNTAIN *et al.* Netherlands, Elsevier, 317–362 (Developments in Geotectonics, 23).

RUTTER, E.H., BRODIE, K.H. and EVANS, P.L. (1993): Structural geometry, lower crustal magmatic underplating and lithospheric stretching in the Ivrea-Verbano zone, northern Italy. J. Struct. Geol., **15**, 647–662.

SANDIFORD, M. (1985): The origin of retrograde shear zones in the Napier Complex: implications for the tectonic evolution of Enderby Land, Antarctica. J. Struct. Geol., **7**, 477–488.

SANDIFORD, M. and WILSON, C.J.L. (1984): The structural evolution of the Fyfe Hills-Khmara Bay region, Enderby Land, East Antarctica. Aust. J. Earth Sci., **31**, 403–426.

SHERATON, J.W., TINGEY, R.J., BLACK, L.P., OFFE, L.A. and ELLIS, D.J. (1987): Geology of Enderby Land and western Kemp Land, Antarctica. BMR Bull., **223**, 51 p.

SHIRAISHI, K., ELLIS, D.J., FANNING, C.M., HIROI, Y., KAGAMI, H. and MOTOYOSHI, Y. (1997): Reexamination of the metamorphic and protolith ages of the Rayner Complex, Antarctica: Evidence for the Cambrian (Pan-Africa) regional metamorphic event. Antarctic Regions: Geological Evolution and Processes, ed. by C. A. RICCI. Siena, Terra Antarct. Publ., 79–88.

SIBSON, R.H. (1975): Generation of pseudotachylyte by ancient seismic faulting. R. Astron. Soc. London J., **43**, 775–794.

TOYOSHIMA, T. (1990): Pseudotachylite from the Main Zone of the Hidaka metamorphic belt, Hokkaido, northern Japan. J. Metamorph. Geol., **8**, 507–523.

TOYOSHIMA, T., KOMATSU, M. and SHIMURA, T. (1994): Tectonic evolution of lower crustal rocks in an exposed magmatic arc section in the Hidaka metamorphic belt, Hokkaido, northern Japan. The Island Arc, **3**, 182–198.

TOYOSHIMA, T., KOMATSU, M. and SHIMURA, T. (1996): Crustal development and tectonics of the Hidaka metamorphic belt, Hokkaido, northern Japan—with reference to the nature of lower crusts, mechanical behavior of arc crusts, formation of crustal-scale décollement and exhumation of deep-crustal rocks—. Tectonics and Metamorphism (The HARA Volume), ed. by T. SHIMAMOTO *et al.* Tokyo, Soubun Co., Ltd., 145–156 (in Japanese with English abstract).

TOYOSHIMA, T., OSANAI, Y., OWADA, M., TSUNOGAE, T., HOKADA, T. and CROWE, W.A. (1998): Deformation of ultrahigh-temperature metamorphic rocks from Tonagh Island, Napier Complex, East Antarctica. The 18th Symposium on Antarctic Geosciences, Program and Abstracts, 20–21 October 1998. Tokyo, Natl. Inst. Polar Res., 27–28 (in Japanese).

TSUNOGAE, T., OSANAI, Y., TOYOSHIMA, T., OWADA, M., HOKADA, T. and CROWE, W.A. (1998): Ultrahigh-temperature mafic granulite from Tonagh Island, Napier Complex. The 18th Symposium on Antarctic Geosciences, Program and Abstracts, 20–21 October 1998. Tokyo, Natl. Inst. Polar Res., 29–30 (in Japanese).

TSUNOGAE, T., OSANAI, Y., TOYOSHIMA, T., OWADA, M., HOKADA, T. and CROWE, W.A. (1999): Metamorphic reactions and preliminary *P-T* estimates of ultrahigh-temperature mafic granulite from Tonagh Island in the Napier Complex, East Antarctica. Polar Geosci., **12**, 71–86.

(Received April 12, 1999; Revised manuscript accepted May 26, 1999)